JOURNAL OF SYNCHROTRON RADIATION
ISSN 1600-5775

A mail-in and user facility for X-ray absorption near-edge structure: the CEI-XANES laboratory X-ray spectrometer at the University of Washington

Alexander S. Ditter,[a] Evan P. Jahrman,[a] Liam R. Bradshaw,[b] Xiaojing Xia,[c] Peter J. Pauzauskie[d,e] and Gerald T. Seidler[a]*

[a]Department of Physics, University of Washington, PO Box 351650, Seattle, WA 98195-1560, USA, [b]Molecular Analysis Facility, University of Washington, 4000 15th Ave NE, Seattle, WA 98195, USA, [c]Department of Molecular Science and Engineering, University of Washington, Seattle, WA 98195, USA, [d]Department of Materials Science and Engineering, University of Washington, 3920 E. Stevens Way NE, Seattle, WA 98195, USA, and [e]Physical and Computational Sciences Directorate, Pacific Northwest National Laboratory, 902 Battelle Blvd, Richland, WA 99352, USA.
*Correspondence e-mail: seidler@uw.edu

Received 31 May 2019
Accepted 16 September 2019

Edited by R. W. Strange, University of Essex, UK

Keywords: XAS; XANES; tabletop; user facility; XAFS; laboratory spectrometer; mail-in XAFS.

There are more than 100 beamlines or endstations worldwide that frequently support X-ray absorption fine-structure (XAFS) measurements, thus providing critical enabling capability for research across numerous scientific disciplines. However, the absence of a supporting tier of more readily accessible, lower-performing options has caused systemic inefficiencies, resulting in high oversubscription and the omission of many scientifically and socially valuable XAFS applications that are incompatible with the synchrotron facility access model. To this end, this work describes the design, performance and uses of the Clean Energy Institute X-ray absorption near-edge structure (CEI-XANES) laboratory spectrometer and its use as both a user-present and mail-in facility. Such new additions to the XAFS infrastructure landscape raise important questions about the most productive interactions between synchrotron radiation and laboratory-based capabilities; this can be discussed in the framework of five categories, only one of which is competitive. The categories include independent operation on independent problems, use dictated by convenience, pre-synchrotron preparatory use of laboratory capability, post-synchrotron follow-up use of laboratory capability, and parallel use of both synchrotron radiation and laboratory systems.

1. Introduction

X-ray absorption spectroscopy (XAS) exhibits a global intellectual reach, with more than 100 endstations or beamlines at synchrotron or free-electron laser facilities world-wide. This has led to continual scientific impact across numerous disciplines (Bunker, 2010; de Groot & Kotani, 2008), with XAS playing an especially central role in research in catalysis (Caudillo-Flores *et al.*, 2018; Thomas & Sankar, 2001), electrical energy storage (McBreen *et al.*, 1988; McBreen, 2009; Cheng *et al.*, 2017; Li *et al.*, 2018), environmental sciences (Ma *et al.*, 2019), fundamental chemistry and physics (Young, 2014), biochemistry (Sarangi, 2013; Porcaro *et al.*, 2018; Kowalska & DeBeer, 2015), and heavy-element chemistry (Kosog *et al.*, 2012; Shi *et al.*, 2014). Much of the highest profile contemporary research does require the full brilliance, time resolution or other extreme performance metrics of these light sources, but a considerable fraction of ongoing excellent work does not. Hence, although the history of XAS at synchrotron facilities is an undisputed scientific success, the recent reinvigoration of laboratory-based XAS after several quiescent decades has been spawned by four observations: (i) the improved spectrometer performance seen with modern

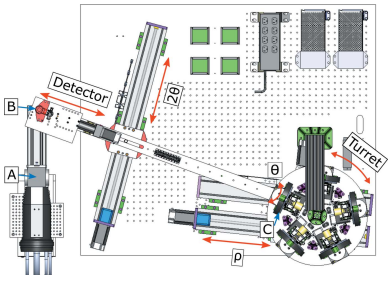

components; (ii) the fact that the synchrotron facilities cannot support the full range of existing demand for XAS; (iii) light source operations could benefit from a supporting tier of higher-access, if lower-performing, XAS capability; and (iv) drawing analogy to X-ray diffraction, there is a large range of 'routine analytical' use of XAS that is largely incompatible with synchrotron facility priorities.

The observation of the possible synergies and mutual benefits from the coexistence of synchrotron facilities and laboratory-based systems is not new, and was recently summarized by Seidler *et al.* (2014). Key unmet opportunities include the broad inclusion of XAS in education, sample validation prior to synchrotron beam time, decreased synchrotron facility oversubscription by providing an alternative venue for experiments not requiring the full beamline performance (*e.g.* many transmission mode studies), rapid-turn-around studies for iterative improvement of new materials synthesis or for industrial process control, and even regulatory applications.

We discuss here a staffed, modern laboratory spectrometer facility for X-ray absorption near-edge structure (XANES) studies in the hard X-ray range. This Clean Energy Institute X-ray Absorption Near-Edge Structure (CEI-XANES) facility is located in the Molecular Analysis Facility (MAF) at the University of Washington (https://www.moles.washington.edu/maf). The MAF is a non-profit cost center which charges a nominal fee to recoup operating costs and operates on a first-come first-served basis. CEI-XANES supports education and academic research at the University of Washington in addition to accepting outside in-person users and providing a mail-in measurement service for academic, national laboratory and industrial studies. Placing this XANES capability in the MAF leads to interesting multi-mode characterization via other capabilities in the MAF, such as X-ray diffraction, various static and dynamic optical wavelength spectroscopies and surface characterization techniques.

An outline of the CEI-XANES technical design was presented a few years ago (Seidler *et al.*, 2016) and the system has been operating since 2016. However, with the full opening of CEI-XANES to outside in-person and mail-in users, we take this opportunity to give a more detailed technical description, to present representative results and to seed a broad discussion of the evolving XAFS infrastructure landscape. Specifically, with the growing number of investigator-owned laboratory spectrometers and also systems run as user facilities, it is time to categorize the different interactions between synchrotron radiation and laboratory-based capabilities. This discussion finds that competition between the two modes is minimal, and that the most prominent interaction between synchrotron radiation and laboratory-based X-ray spectroscopy will probably be disjointed, independent use or else truly synergistic benefits from use of both.

2. Instrument design and operation

The CEI-XANES spectrometer utilizes a Rowland circle monochromator with a fixed source, *i.e.* the so-called 'linear

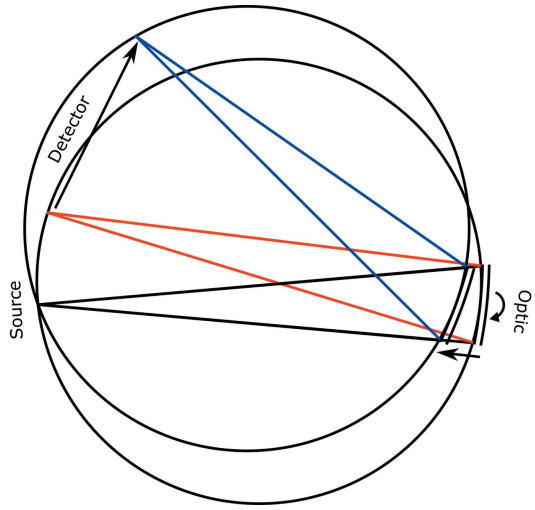

Figure 1
Diagram showing the movement of the detector and the SBCA in a fixed-source Rowland circle in the direction of low (red) to high (blue) energy. Note that both the source position and the direction from the source to the optic are fixed due to the stationary source.

spectrometer' design, well known in the 1970s (Knapp *et al.*, 1978), to produce the tunable monochromatic X-rays needed for XANES measurements. A similar design has recently been implemented in Helsinki (Honkanen *et al.*, 2019), and has seen good use for studies of actinide compounds (Bès *et al.*, 2018) and for a demonstration study for *in situ* catalysis investigations (Moya-Cancino *et al.*, 2019). The relative positioning of key components, *i.e.* source, analyzer and detector, is shown in Fig. 1. The description of the spectrometer then requires two paths: the key components themselves and the supporting components used for motion control. We begin with the former.

The computer-aided design (CAD) rendering in Fig. 2 now provides important context. The X-ray source used in CEI-XANES is re-purposed from a powder X-ray diffractometer. Specifically, it is a repurposed Siemens tube tower system capable of using either a 1.5 kW Ag-anode tube or a 3 kW W-anode tube, just as are used in many powder or single-crystal diffractometers. Two different anode materials are needed to avoid strong fluorescence line contamination, which can occur with the unfortunate position of the W $L\alpha_2$ (8335 eV) emission line in the XANES of Ni (*K*-edge 8333 eV). The X-ray tubes are used in 'point focus' configuration with an effective size of ~0.5 mm (vertical) × 1 mm (in-Rowland-plane) at a median 6° take-off angle. The tube can also be rotated 90° and used in 'line focus', with an effective size of 10 mm (vertical) × 0.5 mm (horizontal), although this results in reduced flux owing to the small detector size. The combination of limited shutter dimension and stronger absorption inside the anode at lower take-off angles results in a beam that slightly 'underfills' the horizontal extent of the spherically bent crystal analyzers (SBCAs; from XRS Tech or else in-house made; Jahrman, Holden, Ditter, Kozimor *et al.*, 2019), which have the required 1 m radius of curvature in the Johann geometry and whose constituent

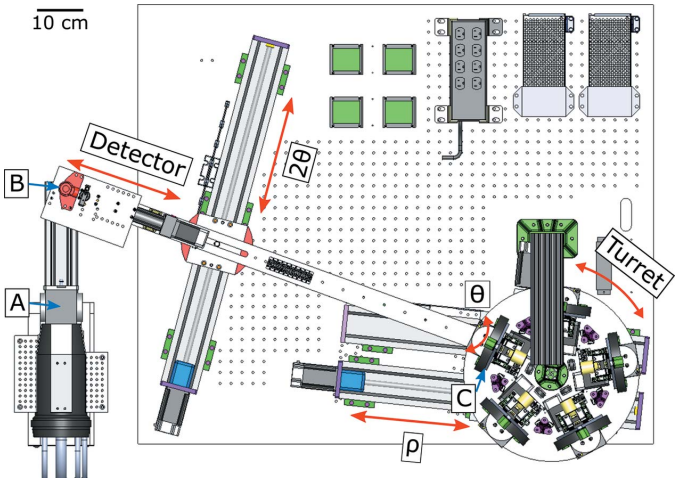

Figure 2
CAD rendering of CEI-XANES (top view). Red arrows indicate the four motors used in a scan (detector, θ, 2θ and ρ) and the turret motor which switches between optics. The key components are labeled with blue arrows and letters: (A) X-ray source, (B) detector and (C) the optic. Not shown is the helium box used to reduce air absorption.

diffracting wafers have 10 cm diameters. A welded aluminium helium space with polyimide windows reduces air absorption on the transit from source to SBCA, and from SBCA to detector. A lead-covered aluminium divider inside the helium box helps to further reduce stray scattering into the line of sight of the detector.

The choice of detector poses particular problems for this generation of high-powered laboratory XAFS systems. First, the peak flux on a sufficiently tall detector can reach from 500 000 s^{-1} to 10^6 s^{-1} and, depending on the choice of SBCA crystal and (*hkl*) orientation, can be accompanied by strong, unwanted harmonics. Second, although toroidal optics useful for laboratory-based XAFS have recently been demonstrated (Jahrman, Holden, Ditter, Kozimor *et al.*, 2019), we still use (spherical) SBCAs, whose sagittal focusing errors result in vertical stretching of the analyzed beam to 25 mm at a Bragg angle of 70°. Hence, a relatively large detector with good energy resolution and high saturation rates would be ideal. We primarily use a silicon drift detector (SDD; Amptek Inc.) with XIA Mercury digital processing hardware. Our SDD has an energy resolution of about 150 eV, which easily rejects any harmonics and most background fluorescence, a necessary property to obtain an accurate measurement. However, the SDD has a collimated area that is just 17 mm^2 and is unable to capture the whole vertical extent of the analyzed beam at lower Bragg angles. The effect of this beam spread on count rates is discussed more thoroughly in our previous work (Jahrman, Holden, Ditter, Kozimor *et al.*, 2019). In addition, the saturation of this SDD above a few hundred thousand counts per second (broadband) sometimes requires beam attenuation to avoid saturation on analyzer harmonics. These limitations could be improved upon with use of a larger, commercially available SDD, and also with use of the latest generation of very high speed processing electronics. All results reported here use the Amptek SDD. We have also investigated the use of a gas proportional counter (GPC; from LND Inc.). The GPC has a large active area (1.5 cm × 4 cm) but an energy resolution $\Delta E \simeq 2$ keV at $E = 7$ keV and so must only be used with low-symmetry optics where the harmonics are well separated, and also requires much greater care in rejecting stray scattering and, for example, fluorescence from the radiation enclosure walls. Using the GPC typically adds to the measurement overhead, as it requires additional background scans with the spectrometer slightly mis-tuned. We note that Honkanen *et al.* (2019) found similar concerns when using a large scintillation detector in their spectrometer.

The final important component of the CEI-XANES instrument is the radiation enclosure. This was fabricated from a welded aluminium frame with lead-lined plywood walls. The total dimensions of the radiation enclosure are quite large (2.5 m × 1.2 m) to allocate space to use the second, opposite shutter on the X-ray tube source for a duplicate but independent spectrometer (Seidler *et al.*, 2016). While the 'B-side' spectrometer is being assembled, we have not yet commissioned it for operations.

Regarding spectrometer motions, a total of four motorized degrees of freedom are needed for energy scanning. We note that we use the 'clock angle' orientation scheme of Mortensen & Seidler (2017) to remove the need for motorizing the SBCA tilt perpendicular to the Rowland plane; the tilt axis is instead adjusted manually *once* with a micrometer and a diverging laser, then is unchanged for any and all SBCA installed onto that apparatus. The remaining four degrees of freedom are the scattering angle of the analyzer as seen by the source (θ; Velmex B59 rotary stage, equipped with a 10:1 gear reducer), the distance from the source to the analyzer (ρ; Velmex tandem BiSlide), a linear translation of the detector assembly to put the detector into the specular reflection condition from the analyzer (2θ; Velmex BiSlide) and a final stage immediately underneath the detector–ample sub-assembly (x; Velmex XSlide) that moves the sample onto the focal point of the monochromated radiation. Including the effect of the reducing gearbox for the 'θ' motor, a single full motor step of the stepper motor results in an angular rotation of 0.004°. For example, near the Fe *K*-edge at 7112 eV using a Ge 620 optic, the minimum step size is approximately 0.1 eV. Although microstepping would, in principal, be able to achieve the same performance, in practice this is not the case: microsteps are highly reproducible across full-step cycles but have irregular spacing within the full step.

In addition to energy scanning, the SBCA turret (see Fig. 3) requires an additional motorized degree of freedom. This five-element turret was included in the 2016 design to allow rapid (approximately 1 min) change of energy ranges, and is fully automated. *This allows for fast changing from one edge to the next without having to open the instrument.* An example of this turret in use is the measurement of several transition metal *K*-edges in an *operando* study of an NMC battery (Jahrman, Pellerin *et al.*, 2019).

Measurements in CEI-XANES are performed by scanning the monochromator over a range of Bragg angles twice, once with the sample in the beam (measuring the transmitted flux)

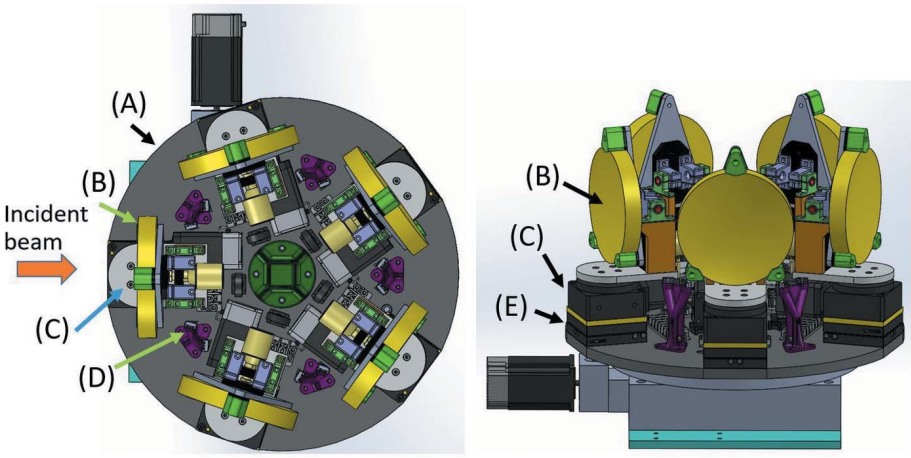

Figure 3
CAD-rendering in top view (left) and perspective view (right). Labeled components are: (A) analyzer turret stage, (B) spherically bent crystal analyzer, (C) theta stage for SBCA tilt stage, (D) limit switches for calibrating theta stages, (E) kinematic mount for easy removal and repositioning of the theta stage with tilt module and SBCA.

and once without the sample in the beam (measuring the incident flux). The absorption is then calculated according to the Beer–Lambert law. This method corrects for any geometrical factors, including the vertical extent of the beam change with the Bragg angle, as well as any low-intensity fluorescence lines in the X-ray tube spectrum. The X-ray tube is set to 20 kV accelerating potential and the current is varied (up to 50 mA) so that the flux on the detector is kept near 50000 counts s^{-1} to avoid detector dead-time. At this count rate, radiation damage is not expected and has never been observed in this instrument. The instrument is operated and data are collected via *Labview*. The data presented here are processed by subtracting a polynomial fit to the pre-edge of the data and normalizing the edge-step to unity using the *DEMETER* package (Ravel & Newville, 2005).

3. Experimental

Lepidocrocite and aboitic magnetite samples were ground to fine powders using a pestle and mortar and then spread over 25 µm-thick polyimide tape. This tape was layered eight times, resulting in a sample with an absorption edge step of approximately 0.5. Synchrotron radiation measurements were performed at beamline 20-BM of the Advanced Photon Source (APS). The spectra were calibrated to an iron foil (EXAFS Materials Inc.). The vanadium reference foil was also from EXAFS Materials Inc.

Single-layer xx3450 pouch cell batteries were manufactured at the Cell Analysis, Modeling and Prototyping (CAMP) Facility at Argonne National Laboratory. The anode used in these cells was Superior Graphite SCL1506T (graphite) and the cathode used was Toda NCM-04ST [$Li(Ni_{0.5}Mn_{0.3}Co_{0.2})O_2$ or NMC532]. The anode was coated onto a 10 µm-thick copper foil for a final electrode loading of 6.38 mg cm^{-2} (coating only). The cathode was coated onto a 20 µm-thick aluminium foil for a final electrode loading of 11.40 mg cm^{-2} (coating only). Other standard pouch cell components included the separator (Celgard 2320), the pouch material (Cellpack-153PL from Youlchon Chemical), and the electrolyte and solvent (1.2 *M* $LiPF_6$ in EC/EMC 3:7 wt%, respectively). Wetting and formation cycles were performed prior to X-ray analysis. The cell exhibited a nominal capacity of 20 mA h. Further cell details can be found in our recent manuscript (Jahrman, Pellerin *et al.*, 2019).

Yb_2O_3 was purchased from Sigma–Aldrich. This powder was mixed with boron nitride powder (BN; Alfa Aesar) and ground using a pestle and mortar, then packed into an aluminium washer between two layers of 25 µm-thick polymide tape. Bulk Yb:$LiYF_4$ was synthesized by the Czochralski process at the University of New Mexico. A piece of a large single crystal was broken off, ground into a fine powder and used to fill the same type of sample holder. Nano-phase Yb:$LiYF_4$ was synthesized at the University of Washington using previously described methods (Roder *et al.*, 2015). The resulting solid was mixed with BN and ground using a pestle and mortar and again put into the same type of sample holder used for the other two Yb-rich samples.

4. Results

Here we describe measurements on several transition metal and rare-earth compounds to demonstrate the utility of CEI-XANES as a user facility. These measurements show that CEI-XANES is able to reproduce synchrotron radiation XAS results and illustrate several 'typical use' cases for measurements.

To make a direct comparison with synchrotron radiation XAS data, lepidocrocite and aboitic magnetite were measured in transmission mode at both CEI-XANES and beamline 20-BM of the APS, as shown in Fig. 4. The CEI-XANES measurements were performed at 20 kV and 10 mA tube power for approximately 2 h each using a Ge (620) optic. Measurement time would have been proportionally decreased with a higher tube current (we used only ∼20% of the maximum power) but we wished to avoid detector saturation. We can see that CEI-XANES reproduces the synchrotron radiation XAS results well, with no discernible difference between spectra, showing that CEI-XANES is capable of producing sufficient quality spectra for many applications. Similar results for Rowland circle spectrometers using SBCA have been reported elsewhere (Seidler *et al.*, 2014; Jahrman, Holden, Ditter, Mortensen *et al.*, 2019; Honkanen *et al.*, 2019).

Fig. 5 shows the measurement of a vanadium foil as well as a comparison with data taken at beamline 13-ID of APS, as per an online XAFS database (GSE-CARS XAFS Spectra Library). In this figure, the APS spectrum is shown both as measured and convolved with a Gaussian with full width at

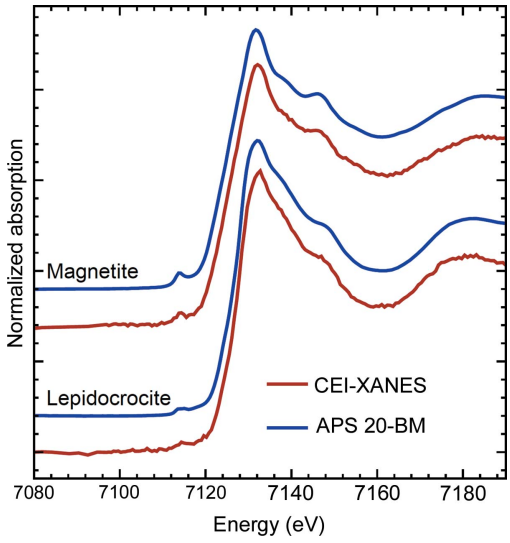

Figure 4
Comparison of CEI-XANES (red) and synchrotron radiation (blue, collected at APS 20-BM) data for both abiotic magnetite (top) and lepidocrocite (bottom). Spectra are offset for clarity. Error bars on the CEI-XANES data due to counting statistics would be approximately the thickness of the plot line.

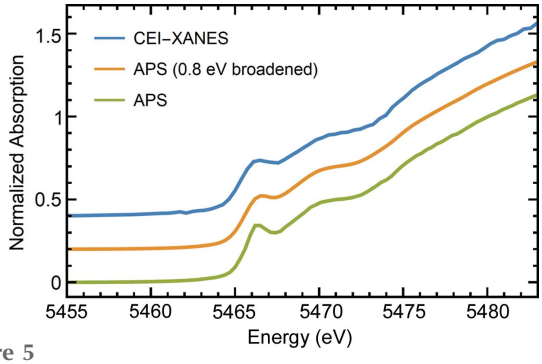

Figure 5
Comparison of vanadium foil *K*-edge XANES spectra taken with CEI-XANES (blue) and at APS (green). Broadening the APS spectrum by 0.8 eV (orange) aligns it well with the CEI-XANES spectrum. Assuming an energy resolution of 0.6 eV for the APS data, we estimate an energy resolution of 1.0 eV for CEI-XANES at the V *K*-edge. Spectra are offset for clarity

half-maximum (FWHM) of 0.8 eV. The broadening of 0.8 eV matches the CEI spectrum, so, taking into account the energy resolution of the initial spectrum (0.6 eV), we estimate the energy resolution of CEI-XANES at the V *K*-edge to be 1.0 eV. This is similar to previous instruments (Jahrman, Holden, Ditter, Mortensen *et al.*, 2019), and, given that the 1*s* core-hole lifetime broadening for transition metals is of the order of 1 eV, this energy resolution is sufficient for many applications. The broadening is likely dominated by the source size in the Rowland plane.

CEI-XANES has its highest flux between 5 keV and 11 keV, so quick measurements of ideal samples at these X-ray energies are possible. We demonstrate this here with a few 2 min scans of the Ni *K*-edge XANES of an NMC pouch cell battery (see Fig. 6). A careful I_0 scan was taken before the study and a longer transmission scan (30 min) was used to normalize the

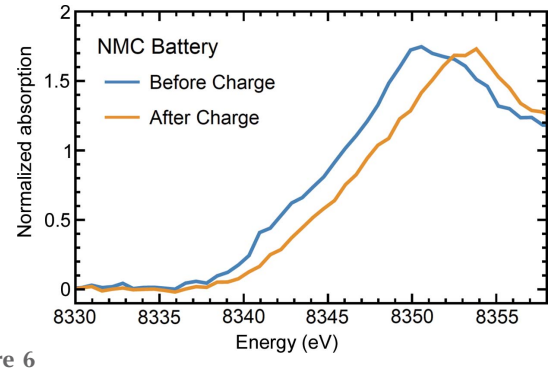

Figure 6
Ni *K*-edge XANES spectra of an NMC pouch cell battery before and after charging. Not shown is a scan over a longer range used to normalize these data. Measurement time was 2 min for each spectrum.

edge step for the quicker 2 min scans. These results are expanded upon elsewhere in a complete *operando* study of pouch cell charging and discharging (Jahrman, Pellerin *et al.*, 2019).

Finally, we report on a 'routine' material characterization example. Ytterbium-doped $LiYF_4$ is an important laser-cooling material (Cittadino *et al.*, 2018); however, when using the Czochralski synthesis, some product crystals could not be cooled upon laser excitation, generating heat instead. One hypothesis is some Yb atoms are reduced to the 2+ oxidation state due to the inclusion of HF in the synthesis, where the strong background absorption by Yb(II) causes the failure of laser cooling. Hence, it is important to learn whether the hydrothermally synthesized nanophase Yb:$LiYF_4$, in which no HF is used, contains Yb(II).

In Fig. 7, bulk and nano-phase Yb:$LiYF_4$ were measured alongside a Yb_2O_3 standard and are presented alongside a previously measured Yb-doped CaF_2 crystal (Yoshida *et al.*, 2005). Previous XANES studies have shown that Yb impurities in calcite and fluorite crystals can be partially in the 2+ oxidation state, and, when they are, a pre-edge peak at 8040 eV is present (Yoshida *et al.*, 2005; Iyer & Peter, 2012; Peter *et al.*, 2012; Rao *et al.*, 1980; Hatwar *et al.*, 1980). This peak is not present for Yb in the 3+ oxidation state and so the absence of these peaks in both the bulk and nanocrystals indicates that Yb is solely in the 3+ oxidation state. This type of routine oxidation-state identification is a common-use case for the CEI-XANES facility, and one that can be easily performed without the brilliance of a synchrotron beamline.

5. Use landscapes in the future with ubiquitous laboratory XAFS and XES

In addition to the present work, there is a growing body of laboratory spectrometers for XAFS and XES in the hard X-ray (Szlachetko *et al.*, 2013; Cohen *et al.*, 1980; Thulke *et al.*, 1983; Tohji *et al.*, 1983; Williams, 1983; Yuryev *et al.*, 2007; Anklamm *et al.*, 2014; Hoszowska *et al.*, 1996; Németh *et al.*, 2016; Kayser *et al.*, 2014; Malzer *et al.*, 2018; Schlesiger *et al.*, 2015; Knapp *et al.*, 1978; Seidler *et al.*, 2014; Jahrman, Holden, Ditter, Mortensen *et al.*, 2019) and tender X-ray ranges

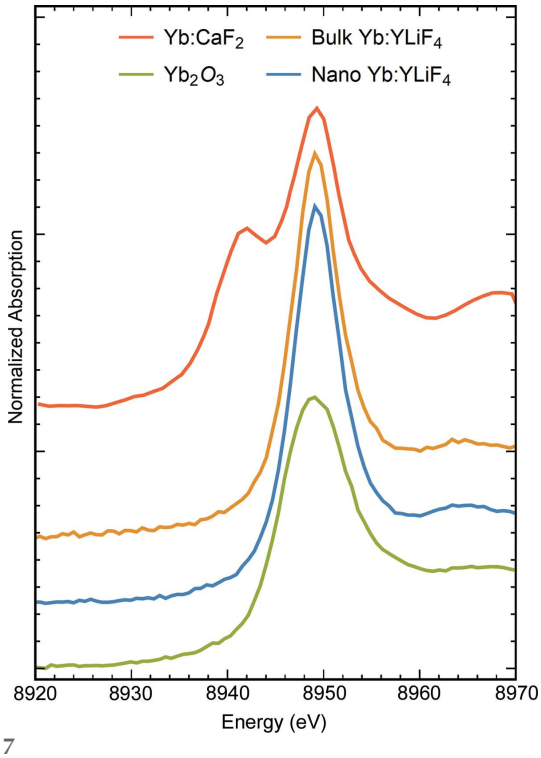

Figure 7
Comparison of nano Yb:$YLiF_4$ crystals (blue) with bulk crystals (yellow), and Yb(III) standard Yb_2O_3 (green) measured at UW and Yb(II/III) mixed-valent Yb:CaF_2 (red) reproduced from the work by Yoshida *et al.* (2005). Spectra are offset for clarity.

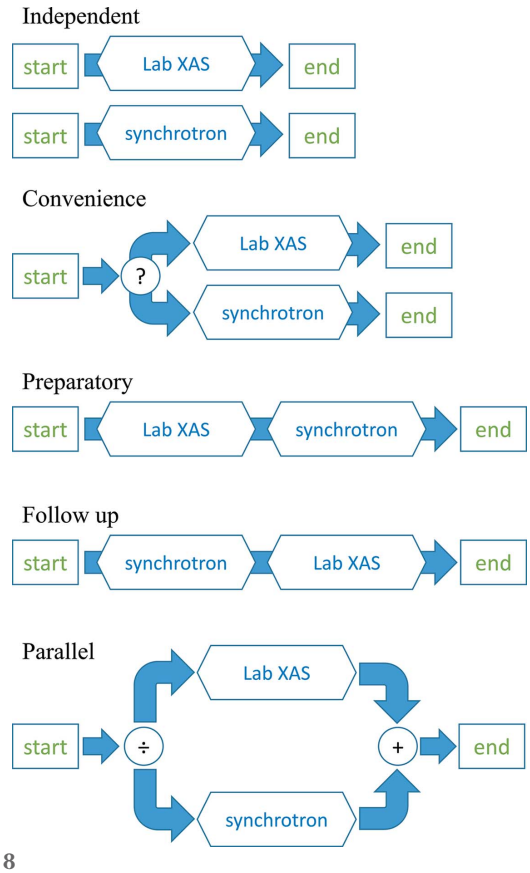

Figure 8
Schema outlining the different ways that synchrotron radiation and laboratory XAS interact. See text for further details.

(Dolgih *et al.*, 1984; Yarmoshenko *et al.*, 1993, 1994, 1995; Sugiura *et al.*, 1972, 1974; Kavčič *et al.*, 2012; Holden *et al.*, 2017). These systems have seen quite varied use, showing an impressive flexibility to address problems in many different fields. For example, the previously mentioned tender X-ray spectrometers have been used to characterize the phosphorous oxidation state in InP quantum dots (Stein *et al.*, 2018) and to look at sulfur speciation in biochars (Holden *et al.*, 2018). The various hard X-ray instruments have been used to look at oxygen vacancies in V_2O_5 (Bi *et al.*, 2019), to work towards creating a standardized regulatory measurement for the Cr oxidation state (Jahrman *et al.*, 2018), to investigate the oxidation state of actinides (Bès *et al.*, 2018) and for a long-duration study of Co/TiO_2 catalysts (Moya-Cancino *et al.*, 2019).

These earliest uses in what appears to be an ongoing rebirth of laboratory XAFS together with the rapidly growing number of laboratory XAFS systems cause us to wonder about the future. We can realistically imagine a time, perhaps ten years hence, when the availability of laboratory XAFS and XES compared with synchrotron radiation XAS has reached a 'sensible' level similar to the relative availabilities of, for example, laboratory-based X-ray diffraction (XRD) compared with synchrotron radiation XRD. In such a world, how should we think about the interplay between laboratory-based and synchrotron capabilities and facilities? Will they compete, be disconnected or be synergistic? Will the synchrotron radiation XAFS demand decrease because of laboratory-based capability, or will it instead greatly increase due to a likely new inclusion of XAFS in university education, with possible discovery of new research applications of XAFS?

While any detailed answers to the above questions would be speculative, we can still identify several important categories of interaction between laboratory and synchrotron XAS, and give exemplars for each. Hence, in Fig. 8 we present five schema, which we now discuss in order. First, there is the situation where the two access paths are fully independent. Independence of laboratory XAS from synchrotron facilities is not due to any lack of technical capability at synchrotron facilities but is instead due to a fundamental mismatch between the character of the desired study and the scientific mission of the synchrotron light source. Rapid feedback studies during new materials synthesis (Stein *et al.*, 2018) and, more hypothetically, industrial quality control testing of, for example, Li-ion battery transition metal oxide electrodes simply do not fit the synchrotron access model: they require a high level of on-demand measurement. On the other hand, the extreme performance characteristics of synchrotron beamlines support a plethora of studies that are impractical or impossible in the laboratory.

Second, there is the category of user convenience. It is only in this access pattern that there is competition between laboratory and synchrotron facilities. The user in this case has

a project that meets the scientific standards of the synchrotron facility so as to pass, for example, peer review by a general user proposal review panel, but the study could be successfully performed with a laboratory spectrometer. At present, the question is one of convenience. As modern laboratory XAS systems and laboratory XAS user and mail-in facilities become more common, it is fair to ask whether the 'question' of operation in this use case may not be in the control of the user but instead in the hands of the synchrotron facility review panel. Some years hence, if there is generically high access to laboratory XAS, then it is fair to expect that synchrotron facilities might be able to decline studies that could be performed with laboratory-based systems.

Third, there are clear benefits from decreasing some of the common inefficiencies ubiquitous in synchrotron radiation XAS beam time usage. Education of new users is an obvious starting point. Although tutorials and workshops have undeniable value, hands-on laboratory-based measurement with iteration in demonstration or pedagogical studies would give a rich training that would immediately increase efficiency for future synchrotron beam time. Furthermore, even experienced users often spend a nontrivial fraction of beam time refining their sample preparation. Much of this work can be done in the laboratory, or at least users can become very highly expert in calculating and executing sample preparation outside of beam time. Finally, the issue of sample and/or experiment design validation must be considered distinct from sample preparation. By validation, we mean any of the following: at least qualitative confirmation of the synthesis of the desired phase; supporting evidence that the intended physical phenomena will indeed have an effect on the to-be-measured spectrum; determination of the efficacy of special sample containers for *e.g.* air-sensitive samples; or evaluation of signal levels to better estimate final beam time needs. This latter case, where one seeks a more accurate estimation of beam time, is where there is considerable ongoing effort (Abe *et al.*, 2018).

Fourth, during post-synchrotron beam time data analysis, users frequently find that some modest additional work would greatly benefit the project, if not in fact be necessary for its completion. If the measurement demands the flux or brilliance of synchrotron radiation, then there is no alternative but to wait for repeat beam time. However, there are at least two obvious cases where laboratory XAS can serve in this regard. First, when XAFS data on additional reference standards are needed, the studies can typically be performed on concentrated samples. Second, XES can often serve to provide added context to aid with interpretation of XANES in particular. This same synergy plays a likely role below, in the final-use case.

Finally, there are likely cases where laboratory-based spectroscopy will strictly enhance synchrotron radiation work at an equal level of scientific merit, rather than merely augmenting in support. The most obvious example is using laboratory-based non-resonant XES to provide direct context for better interpretations of synchrotron-based XANES results. Valence-to-core XES can clearly improve understanding of bonding character without the need to address the subtleties of core-hole effects, and $K\alpha$ XES can sometimes give a cleaner fingerprint of classical oxidation state of the species of interest than XANES, as the former is less sensitive to local environment than the latter (Holden *et al.*, 2018).

6. Conclusions

We have demonstrated the capabilities of the CEI-XANES instrument as the first mail-in XANES user facility using laboratory-based instrumentation, and shown the capability to produce synchrotron-quality spectra in the 5–11 keV range. We have also outlined a number of ways that laboratory systems interact with synchrotron radiation X-ray spectroscopies, and argue that laboratory spectrometers are best seen not as a direct competitor with synchrotron facility operations, but rather as an expansion of the existing XAFS access landscape to become more similar to those of the overwhelming majority of other analytical methods. This will expand the user base especially in the emerging field of 'analytical' applications of XAFS, but will also lead to better prepared and, we can hope, high-impact synchrotron radiation XAFS studies in disciplines where XAFS has not yet made entry. Therefore, the continuing development of laboratory instruments, including user-facility-class instruments like the one described here, are a promising sign for increased access and expansion in the utilization of X-ray absorption spectroscopy.

Acknowledgements

We gratefully acknowledge the help of Maxim I. Boyanov and Kenneth M. Kemmer in providing the iron reference standards and synchrotron radiation XAS measurements at APS 20-BM. We would also like to thank Bryant J. Polzin, Steven E. Trask and Allison R. Dunlop of Argonne for helping to produce the NMC battery.

Funding information

This material is based in part upon work supported by the State of Washington through the University of Washington Clean Energy Institute and via funding from the Washington Research Foundation. EPJ was supported in part by the Joint Center for Energy Storage Research (JCESR), an Energy Innovation Hub funded by the US Department of Energy, Office of Science and Basic Energy Sciences. Part of this work was conducted at the Molecular Analysis Facility, a National Nanotechnology Coordinated Infrastructure site at the University of Washington which is supported in part by the National Science Foundation (grant No. NNCI-1542101), the University of Washington, the Molecular Engineering and Sciences Institute, and the Clean Energy Institute. XX and PJP gratefully acknowledge financial support from the MURI:MARBLe project under the auspices of the Air Force Office of Scientific Research (Award No. FA9550-16-1-0362). This research used resources of the Advanced Photon Source, an Office of Science User Facility operated for the US

Department of Energy (DOE) Office of Science by Argonne National Laboratory, and was supported by the US DOE (contract No. DE-AC02-06CH11357), and the Canadian Light Source and its funding partners.

References

Abe, H., Aquilanti, G., Boada, R., Bunker, B., Glatzel, P., Nachtegaal, M. & Pascarelli, S. (2018). *J. Synchrotron Rad.* **25**, 972–980.

Anklamm, L., Schlesiger, C., Malzer, W., Grötzsch, D., Neitzel, M. & Kanngießer, B. (2014). *Rev. Sci. Instrum.* **85**, 053110.

Bès, R., Ahopelto, T., Honkanen, A.-P., Huotari, S., Leinders, G., Pakarinen, J. & Kvashnina, K. (2018). *J. Nucl. Mater.* **507**, 50–53.

Bi, W., Jahrman, E., Seidler, G., Wang, J., Gao, G., Wu, G., Atif, M., AlSalhi, M. & Cao, G. (2019). *ACS Appl. Mater. Interfaces*, **11**, 16647–16655.

Bunker, G. (2010). *Introduction to XAFS*. Cambridge University Press.

Caudillo-Flores, U., Muñoz-Batista, M. J., Kubacka, A. & Fernández-García, M. (2018). *ChemPhotoChem*, **2**, 777–785.

Cheng, H., Lu, C., Liu, J., Yan, Y., Han, X., Jin, H., Wang, Y., Liu, Y. & Wu, C. (2017). *Prog. Nat. Sci.: Mater. Int.* **27**, 66–73.

Cittadino, G., Volpi, A., Di Lieto, A. & Tonelli, M. (2018). *J. Phys. D Appl. Phys.* **51**, 145302.

Cohen, G. G., Fischer, D. A., Colbert, J. & Shevchik, N. J. (1980). *Rev. Sci. Instrum.* **51**, 273–277.

Dolgih, V. E., Cherkashenko, V. M., Kurmaev, E. Z., Goganov, D. A., Ovchinnikov, E. K. & Yarmoshienko, Y. M. (1984). *Nucl. Instrum. Methods Phys. Res.* **224**, 117–119.

Groot, F. de & Kotani, A. (2008). *Core Level Spectroscopy of Solids*, in *Advances in Condensed Matter Science*. Boca Raton: CRC Press.

Hatwar, T. K., Nayak, R. M., Padalia, B. D., Ghatikar, M. N., Sampathkumaran, E. V., Gupta, L. C. & Vijayaraghavan, R. (1980). *Solid State Commun.* **34**, 617–620.

Holden, W. M., Hoidn, O. R., Ditter, A. S., Seidler, G. T., Kas, J., Stein, J. L., Cossairt, B. M., Kozimor, S. A., Guo, J., Ye, Y., Marcus, M. A. & Fakra, S. (2017). *Rev. Sci. Instrum.* **88**, 073904.

Holden, W. M., Seidler, G. T. & Cheah, S. (2018). *J. Phys. Chem. A*, **122**, 5153–5161.

Honkanen, A.-P., Ollikkala, S., Ahopelto, T., Kallio, A.-J., Blomberg, M. & Huotari, S. (2019). *Rev. Sci. Instrum.* **90**, 033107.

Hoszowska, J., Dousse, J.-C., Kern, J. & Rhême, C. (1996). *Nucl. Instrum. Methods Phys. Res. A*, **376**, 129–138.

Iyer, A. K. & Peter, S. C. (2012). *Eur. J. Inorg. Chem.* **2012**, 1790–1794.

Jahrman, E. P., Holden, W. M., Ditter, A. S., Kozimor, S. A., Kihara, S. L. & Seidler, G. T. (2019). *Rev. Sci. Instrum.* **90**, 013106.

Jahrman, E. P., Holden, W. M., Ditter, A. S., Mortensen, D. R., Seidler, G. T., Fister, T. T., Kozimor, S. A., Piper, L. F. J., Rana, J.,Hyatt, N. C. & Stennett, M. C. (2019). *Rev. Sci. Instrum.* **90**, 024106.

Jahrman, E. P., Pellerin, L. A., Ditter, A. S., Bradshaw, L. R., Polzin, B. J., Trask, S. E., Dunlop, A. R., Fister, T. T. & Seidler, G. T. (2019). *J. Electrochem. Soc.* **166**, A2549–A2555.

Jahrman, E. P., Seidler, G. T. & Sieber, J. R. (2018). *Anal. Chem.* **90**, 6587–6593.

Kavčič, M., Budnar, M., Mühleisen, A., Gasser, F., Žitnik, M., Bučar, K. & Bohinc, R. (2012). *Rev. Sci. Instrum.* **83**, 033113.

Kayser, Y., Błachucki, W., Dousse, J.-C., Hoszowska, J., Neff, M. & Romano, V. (2014). *Rev. Sci. Instrum.* **85**, 043101.

Knapp, G. S., Chen, H. & Klippert, T. E. (1978). *Rev. Sci. Instrum.* **49**, 1658–1666.

Kosog, B., La Pierre, H. S., Denecke, M. A., Heinemann, F. W. & Meyer, K. (2012). *Inorg. Chem.* **51**, 7940–7944.

Kowalska, J. & DeBeer, S. (2015). *Biochim. Biophys. Acta*, **1853**, 1406–1415.

Li, W., Li, M., Hu, Y., Lu, J., Lushington, A., Li, R., Wu, T., Sham, T.-K. & Sun, X. (2018). *Small Methods*, **2**, 1700341.

Ma, B., Charlet, L., Fernandez-Martinez, A., Kang, M. & Madé, B. (2019). *Appl. Geochem.* **100**, 414–431.

Malzer, W., Grötzsch, D., Gnewkow, R., Schlesiger, C., Kowalewski, F., Van Kuiken, B., DeBeer, S. & Kanngießer, B. (2018). *Rev. Sci. Instrum.* **89**, 113111.

McBreen, J. (2009). *J. Solid State Electrochem.* **13**, 1051–1061.

McBreen, J., O'Grady, W. E. & Pandya, K. I. (1988). *J. Power Sources*, **22**, 323–340

Mortensen, D. R. & Seidler, G. T. (2017). *J. Electron Spectrosc. Relat. Phenom.* **215**, 8–15.

Moya-Cancino, J. G., Honkanen, A.-P., van der Eerden, A. M. J., Schaink, H., Folkertsma, L., Ghiasi, M., Longo, A., de Groot, F. M. F., Meirer, F., Huotari, S. & Weckhuysen, B. M. (2019). *ChemCatChem*, **11**, 1039–1044.

Németh, Z., Szlachetko, J., Bajnóczi, É. G. & Vankó, G. (2016). *Rev. Sci. Instrum.* **87**, 103105.

Peter, S. C., Disseler, S. M., Niclas Svensson, J., Carretta, P. & Graf, M. J. (2012). *J. Alloys Compd.* **516**, 126–133.

Porcaro, F., Roudeau, S., Carmona, A. & Ortega, R. (2018). *Trends Anal. Chem.* **104**, 22–41.

Rao, C. N. R., Sarma, D. D., Sarode, P. R., Sampathkumaran, E. V., Gupta, L. C. & Vijayaraghavan, R. (1980). *Chem. Phys. Lett.* **76**, 413–415.

Ravel, B. & Newville, M. (2005). *J. Synchrotron Rad.* **12**, 537–541.

Roder, P. B., Smith, B. E., Zhou, X., Crane, M. J. & Pauzauskie, P. J. (2015). *Proc. Natl. Acad. Sci. USA*, **112**, 15024–15029.

Sarangi, R. (2013). *Coord. Chem. Rev.* **257**, 459–472.

Schlesiger, C., Anklamm, L., Stiel, H., Malzer, W. & Kanngießer, B. (2015). *J. Anal. At. Spectrom.* **30**, 1080–1085.

Seidler, G. T., Mortensen, D. R., Ditter, A. S., Ball, N. A. & Remesnik, A. J. (2016). *J. Phys. Conf. Ser.* **712**, 012015.

Seidler, G. T., Mortensen, D. R., Remesnik, A. J., Pacold, J. I., Ball, N. A., Barry, N., Styczinski, M. & Hoidn, O. R. (2014). *Rev. Sci. Instrum.* **85**, 113906.

Shi, W.-Q., Yuan, L.-Y., Wang, C.-Z., Wang, L., Mei, L., Xiao, C.-L., Zhang, L., Li, Z.-J., Zhao, Y.-L. & Chai, Z.-F. (2014). *Adv. Mater.* **26**, 7807–7848.

Stein, J. L., Holden, W. M., Venkatesh, A., Mundy, M. E., Rossini, A. J., Seidler, G. T. & Cossairt, B. M. (2018). *Chem. Mater.* **30**, 6377–6388.

Sugiura, C., Gohshi, Y. & Suzuki, I. (1972). *Jpn. J. Appl. Phys.* **11**, 911–912.

Sugiura, C., Gohshi, Y. & Suzuki, I. (1974). *Phys. Rev. B*, **10**, 338–343.

Szlachetko, M., Berset, M., Dousse, J.-C., Hoszowska, J. & Szlachetko, J. (2013). *Rev. Sci. Instrum.* **84**, 093104.

Thomas, J. M. & Sankar, G. (2001). *Acc. Chem. Res.* **347**, 571–581.

Thulke, W., Haensel, R. & Rabe, P. (1983). *Rev. Sci. Instrum.* **54**, 277–283.

Tohji, K., Udagawa, Y., Kawasaki, T. & Masuda, K. (1983). *Rev. Sci. Instrum.* **54**, 1482–1487.

Williams, A. (1983). *Rev. Sci. Instrum.* **54**, 193–197.

Yarmoshenko, Y. M., Trofimova, V. A., Dolgih, V. E., Korotin, M. A., Kurmaev, E. Z., Aguiar, J. A., Ferreira, J. M. & Pavao, A. C. (1995). *J. Phys. Condens. Matter*, **7**, 213–218.

Yarmoshenko, Y. M., Trofimova, V. A., Elokhina, L. V., Kurmaev, E. Z., Butorin, S., Cloots, R., Ausloos, M., Aguiar, J. A. & Lobatchevskaya, N. I. (1993). *J. Phys. Chem. Solids*, **54**, 1211–1214.

Yarmoshenko, Y. M., Trofimova, V. A., Kurmaev, E. Z., Slater, P. R. & Greaves, C. (1994). *Physica C*, **224**, 317–320.

Yoshida, T., Kagi, H., Tsuno, H., Ohta, A. & Nomura, M. (2005). *Chem. Lett.* **34**, 852–853.

Young, N. A. (2014). *Coord. Chem. Rev.* **277–278**, 224–274.

Yuryev, Y. N., Lee, H.-J., Park, H.-M., Cho, Y.-K., Lee, M.-K. & Pogrebitsky, K. J. (2007). *Rev. Sci. Instrum.* **78**, 025108.